Self-Assembly of Gold Nanoparticles at the Oil-Vapor Interface: From Mono- to Multilayers

Philip Born, Volker Schön, Susanne Blum, Dominik Gerstner, Patrick Huber, and Tobias Kraus

Langmuir 30 (44)

Self-Assembly of Gold Nanoparticles at the Oil-Vapour Interface: From Mono- to Multilayers

Philip Born[1,4], Volker Schön[2], Susanne Blum[1], Dominik Gerstner[1], Patrick Huber[2,3], and Tobias Kraus[1*]

[1]*INM — Leibniz Institute for New Materials, Campus D2 2, 66123 Saarbrücken, Germany*

[2]*Experimental Physics, Saarland University, Campus E2 6, 66046 Saarbrücken, Germany*

[3]*Institute of Materials Physics and Technology, Hamburg University of Technology (TUHH), Eißendorfer Str. 42, 21073 Hamburg-Harburg, Germany*

[4]*Present address: Institut für Materialphysik im Weltraum, Deutsches Zentrum für Luft- und Raumfahrt, 51170 Köln, Germany*

E-mail: tobias.kraus@inm-gmbh.de

Phone: +49-681-9300-389. Fax: +49-681-9300-279

Abstract

Alkylthiol-coated gold nanoparticles spontaneously segregate from dispersion in toluene to the toluene-vapour interface. We show that surface tension drops during segregation with a rate that depends on particle concentration. Mono- and multilayers of particles form depending on particle concentration, time, and temperature. X-ray reflectometry indicates fast monolayer formation and slow multilayer formation. A model that combines diffusion-limited segregation driven by surface energy and heterogeneous agglomeration driven by dispersive van der Waals particle interactions is proposed to describe film formation.

*To whom correspondence should be addressed

Introduction

Liquid interfaces are natural templates for the self-assembly of nanoparticle films. Fluid interfaces can trap or support particle without lowering their in-plane mobility. Interactions between the particles can then guide them into regular structures. Assembly at liquid-liquid interfaces has been used to prepare ordered films of charged gold nanoparticles,[1] spaced polymer particles,[2] and binary polymer particle mixtures[3] over several cm^2, for example.

Particle assembly at fluid interfaces often requires two liquids and multiple steps. Particles are suspended in an unpolar solvent, placed on an immiscible liquid and arrange at the liquid-liquid or gas-liquid interface. Technologically, one-step processes with a single solvent are more desirable. Industrial coating processes such as slit coating or dip coating can deposit films at high speeds over large areas, but they can only handle a single liquid. One-step, single-solvent processes require dispersions in which particles spontaneously segregate to the interface but do not agglomerate and deposit.

Spontaneous segregation has been reported for evaporating dispersions. In modern coatings applied by the automotive industry, perfluorinated particles segregate to the oil-vapour interface during drying, lower its surface energy and make the coated surface easier to clean.[4] Bigioni *et al.* showed that unpolar gold nanoparticles segregate to the oil-vapour-interface of a drying drop and obtained regular monolayers on the substrate.[5] Friedrich *et al.* studied the structure of assembled semiconductor particle films and suggested that they had formed at the gas-liquid interface.[6] Pietra *et al.* observed the assembly of semiconductor nanorods with in-situ SAXS and confirmed that it occurred at the gas-liquid interface.[7] We are interested in solvent-particle combinations that spontaneously form ordered films with controllable thickness without evaporation.

Spontaneous segregation occurs in the absence of convection if moving a particle to the interface lowers free energy sufficiently to trap the particle. If the deformation of the interface and gravitational effects are neglected, the free energy gain per particle can be estimated from a weighted balance of areas. As a particle moves from the dispersion to the interface, the interfacial area between the particle and its original dispersion medium ("solvent") A_{ps} decreases, the interfacial area between the particle and the third phase ("environment") A_{pe} increases, and the interfacial area between the solvent and the environment A_{se} decreases. The areas depend on the length x by which the particle protrudes into the environment. We obtain the free energy change ΔG by weighting the areas with the corresponding interfacial energies between particle and the environment γ_{pe}, between

particle and solvent γ_{ps}, and between solvent and environment γ_{se}:

$$-\Delta G = (\gamma_{ps} - \gamma_{pe}) \cdot A_{pe}(x) + \gamma_{se} \cdot A_{se}(x) \tag{1}$$

This relation indicates prerequisites for spontaneous segregation. The interfacial energy of particles in the solvent typically is lower than in the environment, and the first term therefore negative. It must be offset by a gain in the interfacial energy between solvent and environment. Since interfacial energies of oil-vapour interfaces are generally lower than that of oil-water interfaces, this requirement is easier to meet — and segregation is more likely to occur — in oil-in-water emulsions than in oil drops in air. Segregation is used in Pickering-Ramsden emulsions, where unpolar particles adsorb at the oil-water interface and stabilize the emulsion droplets.[8] Can it also drive the self-assembly of particle films at the liquid-vapour interface?

We answer this question for dodecanethiol-coated gold nanoparticles (AuNP) with core radii of 4 nm in toluene. Toluene has a higher interfacial energy than dodecane and is a good unpolar solvent. Recent studies indicate a small tendency of AuNP to agglomerate in toluene.[9,10] The particles are known to segregate to hexane-water interfaces[11] and lower the interfacial energy between hexane and water from 53 mJ m^{-2} to 37 mJ m^{-2}.[11] Segregation to the toluene-vapour interface should cause smaller changes.

We studied under which conditions AuNP segregate to the gas-liquid interface and assemble into films. Dispersions with different particle concentrations were characterized using surface tensiometry on hanging drops, electron microscopy, and x-ray reflectometry. Kinetics were recovered from time-dependant surface energies, optical reflectometry, and x-ray reflectometry. The small energy differences between dispersed particles, particles trapped at the solvent-vapour interface, and agglomerated particles were probed using x-ray reflectometry at different temperatures.

Results and discussion

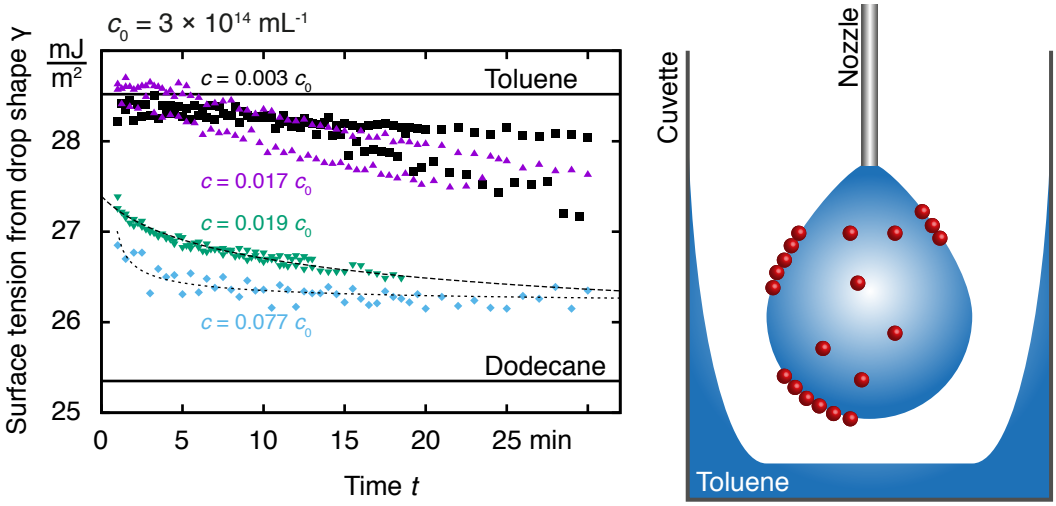

Figure 1: Surface tension evolutions of particle-containing toluene drops in saturated vapour. Each symbol represents a concentration, each trace the changing shape of a single drop that was photographed and fit by a Young-Laplace model to calculate its interfacial energy. Horizontal lines indicate the interfacial energies of pure toluene and dodecane, dashed black lines are fits to a diffusion-limited transport model. The drops were hanging from a vertical nozzle that protruded into a cuvette filled with saturated vapour as shown on the right.

When particles segregate to the toluene-vapour interface and expose the dodecanethiol ligands to the vapour, interfacial energy should drop from the toluene-vapour value[12] of 29 mJ m^{-2} towards the 26 mJ m^{-2} of dodecane.[12] We used hanging drop tensiometry in saturated toluene vapour (Figure 1) to observe this change.

The interfacial energies of hanging drops containing particles consistently decreased with time (Figure 1). Initial values for higher particle concentrations were below that of pure toluene because our measurements were too slow to capture the initial, fast particle segregation. Final values were above that of dodecane and depended on particle concentration, where higher concentrations generally led to lower interfacial energies. Changes became very slow after 20 min, and drops often detached around that time. We did observe some drops (data not shown) that reached interfacial energies close to that of dodecane. The evolution was consistent both with concentration-dependant saturation behaviour (where the surface coverage would depend on particle concentration) and slow segregation kinetics.

If we assume a maximum packing density of 91% (the densest packing of disks) for the particles at the interface and use the known hydrodynamic radius of the particles of 4 nm,

the largest drop in free energy per particle observed was on the order of 1×10^{-19} J, or $30\,k_B T$ at standard conditions. This is on the order of the $\approx 15\,k_B T$ per particle calculated using equation (1) with literature values for interfacial energies[12] and a contact angle of toluene on dodecanethiol-coated gold of 36°. We conclude that interfacial energy is a sufficient driving force for particle segregation to the interface.

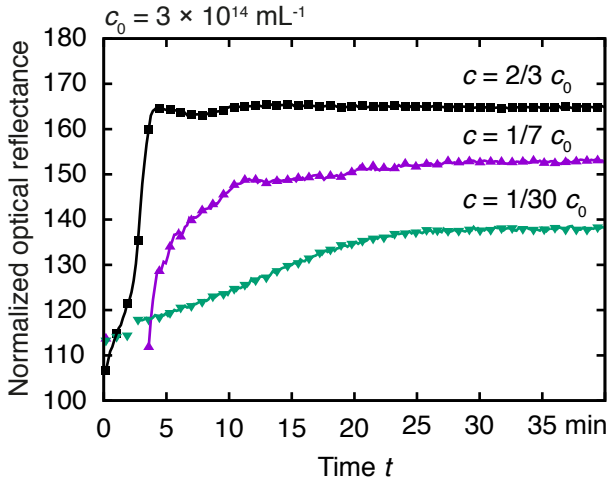

Figure 2: Optical reflectivity of a horizontal toluene-vapour interface at surface plasmon resonance frequency (570 nm). Gold nanoparticles segregated from the dispersion to the interface during the measurement. The layers appeared red-black with a golden sheen to the naked eye. Reflectance values normalized to a particle-free toluene interface. Initial fluctuations are due to focusing.

Visually, particle films at the interface appeared red-black with a golden sheen. The colour seemed stronger at higher particle concentrations. Time-resolved measurement of the optical reflectivity of the planar interface of bulk dispersions (Figure 2) confirmed that the reflectivity at a central wavelength of 570 nm increased with a rate and up to a plateau value that depended on particle concentration (the full spectral evolution of the reflectivity is included in the Supporting Information). Segregation at higher concentrations was so fast that the optical reflectometry did not capture the initial rise. Reflectivity at the lowered concentrations increased with time constants comparable to that of the interfacial energy decrease.

The different plateau levels of reflectivity imply a concentration-dependant density or thickness of the particle film. Particle concentrations were so high that one would expect (from tensiometry) the formation of at least a monolayer in all experiments. The differences in reflectivity cannot be caused by different surface coverages, they can only be explained by particles added beyond a single monolayer. We conclude that multilayer particle films formed with a constant thickness that depended on particle concentration.

They appeared as continuous slabs with a high refractive index and reflected light depending on their thickness. Note that densely packed monolayers of metal particles with coupled surface plasmons are known to appear mirror-like;[13] we believe that the spacing caused by the unpolar ligands reduces the coupling in the layers formed here.

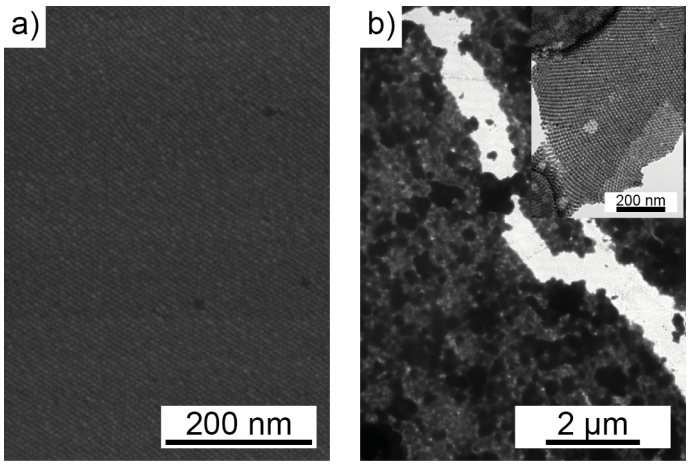

Figure 3: Particle films formed at toluene-vapour interfaces: (a) scanning electron micrograph of a silicon surface on which a toluene drop with a low particle concentration had evaporated, (b) transmission electron micrographs of particle layers transferred from the gas-liquid interface of a high concentration dispersion onto a microscopy grid. The inset shows a crystalline bilayer formed on a different drop.

Particle multilayers are not easily recognized in electron micrographs of dried drops. Depending on particle concentration, dispersed particles may be trapped under the moving gas-liquid interface that already carries a monolayer while drying. A multilayer forms that was not present in the liquid. We often found monolayers (Figure 3 (a)) when drying liquid drops of low particle concentration.[5] In toluene containing high particle concentration, we often found multilayers when we transferred the visible particle film from the interface onto carbon films (Figure 3 (b)). Thick particle films even formed in saturated solvent vapour where evaporation was suppressed.

We observed layer formation *in situ* by X-rays at different particle concentrations and temperatures. X-Ray reflectometry probes the electron density profile normal to the gas-liquid surface, from which layering can be reconstructed.[14] A fit of the x-ray reflectivity at low particle concentrations (Figure 4) reconstructs the surface-normal electron density shown in panel (b). The peak at $z = 0$ indicates a particle layer that formed at the gas-liquid interface at all temperatures. Its electron density is consistent with a densely packed layer of gold cores of the used diameter. The second, smaller peak that is more pronounced at lower temperatures suggests that particles accumulated below the topmost layer. This sub-surface layer was less dense than the top layer and virtually van-

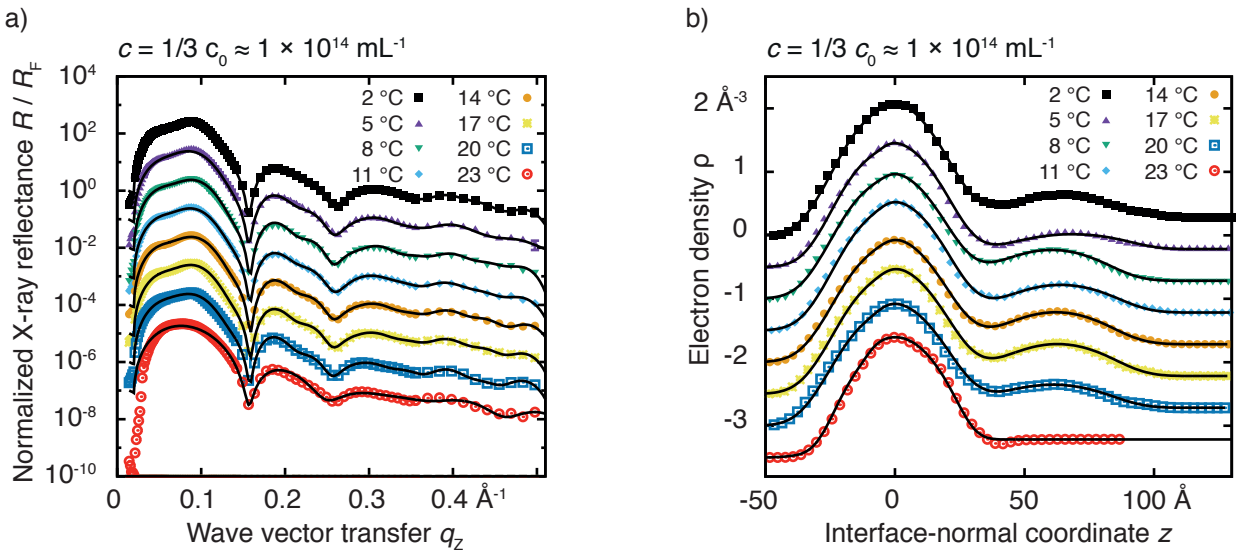

Figure 4: (a) X-ray reflectivity and (b) derived surface electron density profiles of a horizontal toluene-air interface. Gold nanoparticles dispersed in toluene segregated to the interface. A sparse subsurface layer is visible as a peak emerging at lower temperatures. Reflectivity was normalized by the toluene Fresnel reflectivity R_F and plotted as a function of the wavevector transfer parallel to the surface normal q_z.

ished at 23 °C. Note that x-ray reflectrometry averaged over an x-ray spot with an area in the range of centimetres. It is possible (and likely) that the sub-monolayers consisted of disjoint islands of densely packed particles.

The reflectograms allowed us to estimate the top layer density using a simple geometrical model (see below). Its surface coverage depended on the bulk nanoparticle concentration and followed a Langmuir isotherm:

$$\Gamma(c) = \Gamma_\infty \frac{K \cdot c}{1 + K \cdot c} \tag{2}$$

At a temperature of $T = 20\,°\mathrm{C}$, the surface coverage at a bulk particle concentration of $c = 2\,c_0 \approx 6 \times 10^{14}\,\mathrm{mL}^{-1}$ corresponds to a dense packing of particles separated by the ligand layer on the particle surface. By fitting the concentration dependence of the surface coverage (see Supporting Information) we obtained the Langmuir parameters $\Gamma_\infty = (5.8 \pm 0.2) \times 10^{15}\,\mathrm{m}^{-2}$ and the surface activity $K = (2.0 \pm 0.3) \times 10^{-19}\,/\mathrm{m}^3$. Assuming a thermally activated binding mechanism, the difference between bulk and surface energy corresponds to an energy gain on the order of $10\,k_B T$ per particle bound at the surface, in good agreement with the surface-energy based estimates above.

If the particles' segregation to the interface follows a Langmuir adsorption isotherm and transport is purely diffusional, kinetics should follow the transport model of Kral-

chevsky and Nagayama.[16] We estimated the particles' diffusivity using the Einstein-Smoluchovski-Equation as $D = 8.8 \times 10^{-11}\,\mathrm{m^2\,s^{-1}}$ and calculated a characteristic time scale as a function of bulk particle concentration c,

$$\tau(c) = \frac{1}{D}\left(\frac{\partial \Gamma}{\partial c'}\right)^2_{c'=c} \tag{3}$$

that characterizes the time required for a new interface to form. The reduction of interfacial energy can then be expressed as

$$\sigma(t) = \sigma_\mathrm{f} + (\sigma_0 - \sigma_\mathrm{f})\, e^{\frac{t}{\tau(c)}} \operatorname{erfc}\left(\sqrt{\frac{t}{\tau(c)}}\right), \tag{4}$$

where σ_0 is the interfacial energy of the undisturbed liquid surface, σ_f the equilibrium value for a given concentration and $\operatorname{erfc}(x)$ the complementary error function. The broken lines in Figure 1 represent fits of the model to the changing interfacial energy. It was necessary to correct for the initial delay in measurement and to choose a final interfacial energy to fit the data. The characteristic time scale that is set by the Langmuir isotherm parameters and the hydrodynamic particle diameter fits the data without adjustment.

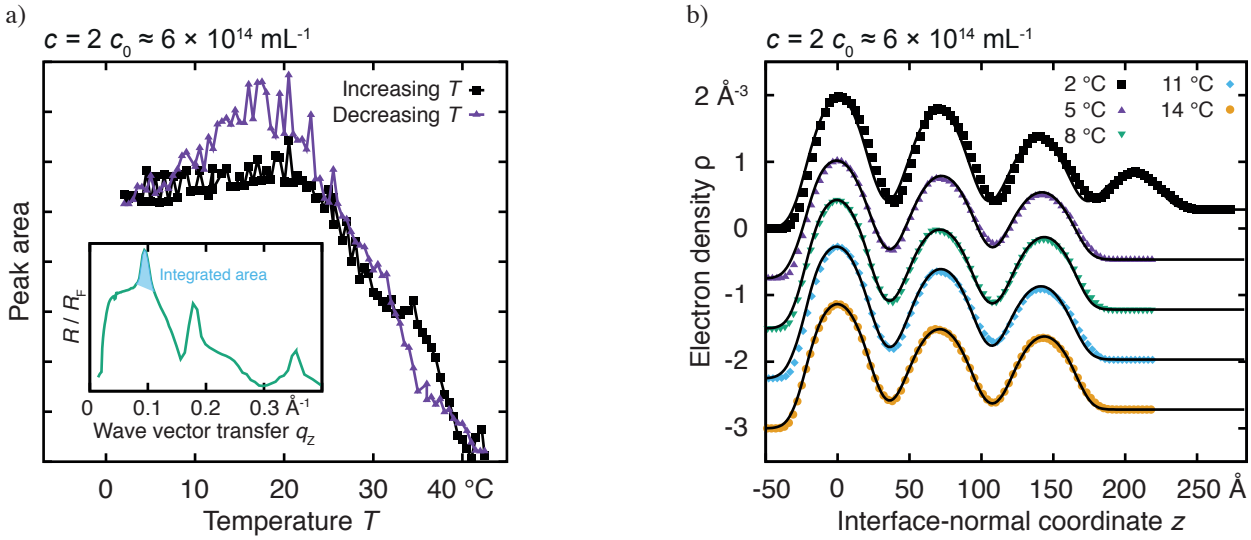

Figure 5: (a) Temperature dependence of the sub-surface x-ray reflectivity and (b) the derived electron density at increased particle concentrations in toluene. Each point in (a) represents the integrated intensity over a 25 min measurement and the indicated angular range. The temperature was changed in 0.5 °C steps. Full x-ray reflectivities were taken at selected temperatures and fit to obtain the electron densities shown in (b).

At higher particle concentrations, additional sub-surface particle layers formed. We

observed up to three layers below the interface (Figure 5 (b)) for $c = 2\,c_0 \approx 6 \times 10^{14}\,\mathrm{mL}^{-1}$ depending on temperature and time. The degree of particle accumulation at decreasing temperatures is indicated in Figure 5 (a). Integration of the x-ray intensity scattered by sub-surface particles indicated accumulation only below 40 °C. The sub-surface accumulation was fully reversible and the films dissolved upon temperature increase until only a monolayer remained. No particles were detected below the interface above 40 °C. The particle layer at the gas-liquid interface remained stable throughout the accessed temperature range.

Temperature-reversible agglomeration has been observed in the bulk for similar particles in linear alkane dispersion.[10] Heterogeneous agglomeration — the addition of particles to pre-existing agglomerates — occurs with a higher probability than homogeneous agglomeration from dispersed particles. In the case of gas-liquid interfaces, a segregating particle layer can act as a nucleation seed. The metastable particle suspension agglomerates underneath the particle monolayer at the interface.

Conclusions

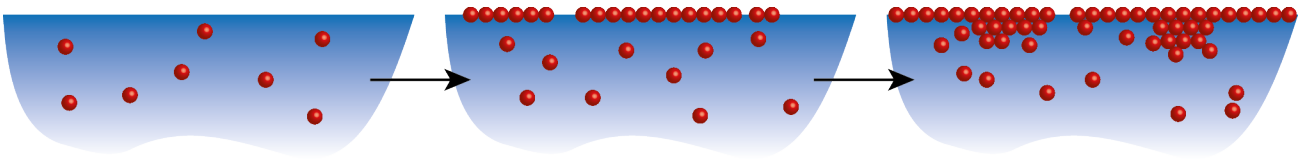

Figure 6: A two-step model for particle film formation. A dense particle layer rapidly forms at the gas-liquid interface and lowers its free energy. Slower, heterogeneous agglomeration is nucleated by this layer and leads to temperature-dependant, reversible growth of less well-defined subsurface layers.

At least four mechanisms can contribute to particle film formation in this system:

1. Monolayer formation at the interface driven by interfacial energy,
2. heterogeneous agglomeration nucleated by the interface layer,
3. homogeneous agglomeration in the bulk,
4. convective transport towards the interface.

The relevant quantities — interfacial energies, interparticle potential, and Péclet number — are in a range such that all four mechanisms can become relevant, depending on particle concentration and temperature.

Monolayer formation appears to be diffusion-limited in a temperature range between 2 °C and 23 °C. The particles lower the interfacial energy of the suspension. In contrast to Pickering-Ramsden emulsions, the energy gain is so small that surface coverage depends on bulk particle concentration. Once the particles have segregated to the interface, they interact through dispersive attractions. It is unclear how large this contribution is compared to the interfacial energy decrease, but we believe that it is small, probably $< 10 k_B T$ per particle.

Particles that are confined at the gas-liquid interface can induce heterogeneous agglomeration. Free particles interact with one or multiple confined particles and adhere to them. This process is strongly temperature-dependant, suggesting even smaller free energy differences. We believe that the stiction probability between particles from the bulk and the monolayer is below that between free particles and the gas-liquid interface. At low concentrations, heterogeneous agglomeration is much slower than monolayer formation. They occur sequentially under typical experimental conditions.

At high concentrations, temperature-dependant homogeneous agglomeration in bulk is expected.[10] The agglomerates can adsorb underneath the topmost particle layer. Larger agglomerates that do not adsorb will sediment and reduce the particle concentration.

Evaporation was suppressed in this study. In an evaporating drop, transport to the interface is enhanced, and fragile agglomerate structure may decompose. The increasing particle concentration in the shrinking drop complicates the situation further. A rough estimate based on Figures published by Bigioni *et al.*[5] (where the interface of a 10 µL drop shrinks with 1.6 µm s^{-1} and the particle diffusion constant is 73 μm^2 s^{-1}) suggests a Péclet number around 40 for an evaporating sessile drop of particle-containing toluene. Under such conditions, evaporation dominates transport. Interface-driven segregation will still be an important mechanism, probably enhanced by the rapid transport of particles to the surface. In the experiments by Bigioni *et al.* with comparatively low particle concentrations, evaporation probably enhances transport to the interface to such a rate that the (slower) agglomeration under the film does not occur before the drop has evaporated.

Particle deposition from thin liquid films becomes hard to control for very small particles. Other methods require precise control of particle concentration to obtain a defined layer thickness. Spontaneous segregation is a simple alternative that works in a large temperature and concentration range. It is a robust process with a free energy gain of around $10 k_B T$ per particle. The energy difference between spontaneous segregation and agglomeration in the bulk (on the order of $k_B T$[10]) can be used to control thickness and morphology of the particle films by ambient temperature.

It remains an open question whether the particles agglomerating below the interfa-

cial monolayer can self-assemble into regular superstructures. In bulk agglomeration, alkanethiol-coated gold nanoparticles form ordered or disordered agglomerates depending on temperature.[17] Grazing incidence small angle X-ray scattering studies in different solvents and at different temperatures could illuminate this point. This question is relevant to many particle assembly experiments that are not strictly bulk: it is often not clear whether assembly took place in the bulk liquid or at and below the interface.

Experimental methods and materials

Nanoparticle synthesis and characterization: Unpolar gold nanoparticles were prepared using a procedure derived from Zheng *etal.*[18] An organic gold complex was thermally decomposed in the presence of an amine-borane complex and dodecane thiol. Typically, 310 mg chlorotriphenylphosphine gold ($AuPPh_3Cl$, ABCR 98 %) were dissolved in 50 mL benzene (Riedel-de-Hahn >99.5 %) to form a colourless solution. For reduction, 530 mg tert-butylamineborane (Fluka 97 %) and 340 mg dodecanethiol (Fluka >98 %) were added and the mixture was heated to 55 °C. The reaction yielded a red particle suspension that was purified by precipitation with ethanol, centrifugation, and resuspension of the particles in toluene. Gold contents of the particle dispersions were measured with an inductively coupled plasma atomic emission spectrometer (ICP-AES, Horiba Jobin Yvon Ultima 2).

Gold core sizes were obtained from transmission electron micrographs made on a Philips CM200 transmission electron microscope (TEM) operating at 200 keV. A drop of suspension was dried on a carbon-coated TEM grid; approximately 400 particles were sized using the ImageJ-software.[19] Hydrodynamic radii are from dynamic light scattering (DLS) performed on a Wyatt Technology DynaPro Titan with a laser emitting at 831 nm. All autocorrelation curves were averaged over 10 measurements and evaluated using a cumulant fit.

Pendant drop tensiometry in saturated vapor: A commercial surface tension measurement setup (G2, Krüss, Hamburg, Germany) was used in pendant drop geometry. For each measurement, toluene containing well-dispersed gold nanoparticles at a known concentration was filled into a syringe. A pendant drop was formed at the tip of a needle that protruded vertically into a cuvette. Toluene covered the bottom of the cuvette and guaranteed a saturated vapour atmosphere (see Figure 1).

We recorded the evolution of the drop with a digital greyscale camera for 30 min. The first minute was discarded to minimize the influence of drop formation. Images were

taken at an interval of 15 s for the first 20 min and at an interval of 30 s for the last 10 min. All images were analyzed using the DSA 2 software provided by Krüss. A Young-Laplace fit was used for every drop to infer the interfacial energy from its shape.

Small changes in surface energy are a challenge in hanging drop experiments. The setup was not temperature-stabilized and operated in the usual range of laboratory temperature fluctuations, causing unexpected interfacial energy differences between drops having similar particle concentration. Vibration probably caused local motion at the gas-liquid interface and altered particle structures. We repeated each measurement several times and excluded cases with jumps and experiments where the volume of the drop changed. All measurements ended when the drop detached or after 1800 s.

Optical reflectometry: We measured the reflectance of the toluene-air interface with an Ocean Optics USB2000 fibre optic spectrometer and and halogen bulb as light source. The measurements covered wavelengths from 400 nm to 950 nm. Halogen light was coupled into a bifurcated fibre cable which picked up the reflected light in backscattering direction. The reflectance of pure toluene was taken as a reference to normalize all intensities.

For each measurement, a beaker was filled almost completely with roughly 10 mL of suspension, immediately covered with a microscopy cover slide and placed underneath the vertically aligned fibre. Measurements were taken at every second for 24 h. The reflectivity reached plateau levels after $\approx$ 30 min or earlier depending on particle concentration.

We analysed the change of reflectivity at the surface plasmon resonance wavelength of the particles. We believe that highest sensitivity is gained at this wavelength.

X-Ray reflectometry and analysis X-ray reflectometry was used to probe the vertical electron density of the particle-laden gas-liquid interface. The short X-ray wavelength used in X-ray reflectometry makes the technique sensitive to structural length scales well below one nanometer. A beam diameter of approximately 1 cm caused lateral averaging.

We used a home-built X-ray reflectometer, where the incident angle, height of the sample, detection path and the detected angle were controlled by stepper motors. A 2.2 kW Cu-Anode from Seifert Analytical X-ray equipped with a multilayer mirror operated in line focus, the beam was further conditioned with motorised slits and attenuators. Samples were enclosed in a sealed cell with built-in temperature control to avoid temperature gradients or evaporation-induced convection. Motorized detector slits allowed adjustment of the angular acceptance of the proportional counter detector from Seifert Analytical. Evacuated flight tubes reduced air scattering on the beam paths between sample and source and detector.

The intensity of X-rays reflected off a structured surface depends on the Fresnel reflectivity of the unstructured surface, modulated with the Fourier transform of the electron density gradient perpendicular to the surface. A thin layer on top additionally scatters photons, leading to interferences between the X-rays scattered from the interfaces. Electron density profiles were obtained through fitting of the angle-dependent reflected X-rays using the *StochFit* package by Stephen Danauskas from the University of Chicago.[20] Particle monolayers at the surface were modelled assuming a hexagonally ordered layer with variable lattice constant of thiol-covered gold particles in a toluene environment and their respective electron densities.[21]

To model the electron density of a particle film, we assumed a hexagonally ordered film of gold cores with a dodecanethiol layer on top and their respective electron densities. We adjust for different surface coverages by changing the lattice constant, larger values lead to a reduced particle density in the surface film. The vertical structure of the particle layer embossed on the liquid surface and thermal fluctuations around the equilibrium height are taken into account.

Acknowledgements

We thank Anika Weber for the synthesis and characterization of gold nanoparticles, John Aveson for tensiometry measurements and useful discussions, and Eduard Arzt for his continuing support. Part of this work was funded by the Deutsche Forschungsgemeinschaft (DFG).

Notes and References

(1) Reincke, F.; Hickey, S.; Kegel, W.; Vanmaekelbergh, D. *Angewandte Chemie, International Edition* **2004**, *43*, 458–462.

(2) Isa, L.; Kumar, K.; Mueller, M.; Grolig, J.; Textor, M.; Reimhult, E. *ACS Nano* **2010**, *4*, 5665–5670.

(3) Vogel, N.; de Viguerie, L.; Jonas, U.; Weiss, C. K.; Landfester, K. *Advanced Functional Materials* **2011**, *21*, 3064–3073.

(4) Chattopadhyay, D. K.; Raju, K. V. S. N. *Progress in Polymer Science* **2007**, *32*, 352–418.

(5) Bigioni, T.; Lin, X.; Nguyen, T.; Corwin, E.; Witten, T.; Jaeger, H. *Nature Materials* **2006**, *5*, 265–270.

(6) Friedrich, H.; Gommes, C. J.; Overgaag, K.; Meeldijk, J. D.; Evers, W. H.; de Nijs, B.; Boneschanscher, M. P.; de Jongh, P. E.; Verkleij, A. J.; de Jong, K. P.; van Blaaderen, A.; Vanmaekelbergh, D. *Nano Letters* **2009**, *9*, 2719–2724.

(7) Pietra, F.; Rabouw, F. T.; Evers, W. H.; Byelov, D. V.; Petukhov, A. V.; Donega, C. d. M.; Vanmaekelbergh, D. *Nano Letters* **2012**, *12*, 5515–5523.

(8) Ramsden, W. *Proceedings of the Royal Society of London* **1903**, *72*, 156–164.

(9) Goubet, N.; Portales, H.; Yan, C.; Arfaoui, I.; Albouy, P.-A.; Mermet, A.; Pileni, M.-P. *Journal of the American Chemical Society* **2012**, *134*, 3714–3719.

(10) Born, P.; Kraus, T. *Physical Review E* **2013**, *87*.

(11) Lacava, J.; Ouali, A.-A.; Raillard, B.; Kraus, T. *Soft Matter* **2014**, *10*, 1696–1704.

(12) Jasper, J. J. *Journal of Physical and Chemical Reference Data* **1972**, *1*, 814–1009.

(13) Remacle, F.; Collier, C.; Heath, J.; Levine, R. *Chemical Physics Letters* **1998**, *291*, 453–458.

(14) Als-Nielsen, J.; McMorrow, D. *Elements of Modern X-Ray Physics*; Wiley-VCH, 2011.

(15) Krachevsky, P. A.; Nagayama, K. In *Particles at Fluid Interfaces and Membranes*; Möbius, D., Miller, R., Eds.; Elsevier, 2001.

(16) Ref. 15, p. 39.

(17) Geyer, T.; Born, P.; Kraus, T. *Physical Review Letters* **2012**, *109*, cited By (since 1996)5.

(18) Zheng, N.; Fan, J.; Stucky, G. *Journal of the American Chemical Society* **2006**, *128*, 6550–6551.

(19) Schneider, C. A.; Rasband, W. S.; Eliceiri, K. W. *Nature Methods* **2012**, *9*, 671–675.

(20) Danauskas, S. M.; Li, D.; Meron, M.; Lin, B.; Lee, K. Y. C. *Journal of Applied Crystallography* **2008**, *41*, 1187–1193.

(21) Schoen, V. X-ray investigations of mesoscopic films at liquid/vapor interfaces. Ph.D. thesis, Saarland University, 2013.